Science of the Total Environment 619–620 (2018) 301–310

Contents lists available at ScienceDirect

Science of the Total Environment

journal homepage: www.elsevier.com/locate/scitotenv

# Hydrochemical controls on reservoir nutrient and phytoplankton dynamics under storms

Nengwang Chen [a,*], Qiongli Mo [a], Yi-Ming Kuo [b], Yuping Su [c], Yanping Zhong [a]

[a] Key Laboratory of the Coastal and Wetland Ecosystems, Fujian Provincial Key Laboratory for Coastal Ecology and Environmental Studies, College of the Environment and Ecology, Xiamen University, Xiamen 361102, China
[b] School of Environmental Studies, China University of Geosciences, Wuhan 430074, China
[c] College of Environmental Science and Engineering, Fujian Normal University, Fuzhou, 350007, China

## HIGHLIGHTS

- Hydrochemical controls on reservoir nutrient and phytoplankton were examined.
- $NH_4$-N and DRP enriched from storm runoff but removed by phytoplankton.
- Chl-*a* variation was mainly controlled by turbidity, $NH_4$-N, DRP, TP and discharge
- The Cyanophyta bloom was fueled by phosphate and ammonium rather than nitrate.

## GRAPHICAL ABSTRACT

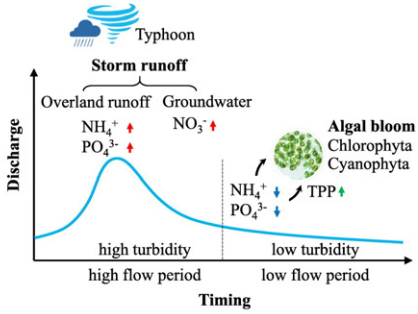


**Reservoir nutrient and phytoplankton response to storms**

## ARTICLE INFO

*Article history:*
Received 23 May 2017
Received in revised form 20 September 2017
Accepted 20 September 2017
Available online 29 November 2017

Editor: Ouyang Wei

*Keywords:*
Nutrient
Storm
Algal bloom
Dynamic factor analysis
Jiulong River
Climate change

## ABSTRACT

Eutrophication and undesired algal blooms in surface water are common and have been linked to increasing nutrient loading. Effects of extreme events such as storms on reservoir nutrient and phytoplankton remain unclear. Here we carried out continuous high-frequency measurements in a long and narrow dam reservoir in southeast China during a storm period in June–July 2015. Our results show a strong nutrient-phytoplankton relationship as well as a very rapid response to storm runoff. We observed an increase in total suspended matter (TSM), ammonium ($NH_4$-N), and dissolved reactive phosphate (DRP), with a sharp decline in chlorophyll-*a* (Chl-*a*) in the high flow periods. Afterward, Chl-*a*, total phytoplankton abundance and Cyanophyta fraction elevated gradually. Nitrate was diluted at first with increasing discharge before concentration increased, likely following a delayed input of groundwater. Physiochemical parameters and Chl-*a* were evenly distributed in the water column during the flooding period. However, 10% of $NH_4$-N and 25% of DRP were removed in surface water (0–1 m) when an algal bloom (Chl-$a > 30\ \mu g\ L^{-1}$) occurred 10 days after peak discharge. Conversely, total particulate P (TPP) of surface water was 58% higher than in the deeper water. Dynamic factor analysis (DFA) revealed that TSM, $NH_4$-N, DRP, total P and discharge significantly explain Chl-*a* variations following storms ($C_{eff} = 0.89$). These findings highlight that the reservoir ecosystem was vulnerable to pulse input from storm runoff and the Cyanophyta bloom was likely fueled by phosphate and ammonium rather than nitrate.



* Corresponding author at: College of the Environment and Ecology, Xiamen University, Xiamen 361102, China.
*E-mail address:* nwchen@xmu.edu.cn (N. Chen).

http://dx.doi.org/10.1016/j.scitotenv.2017.09.216
0048-9697/

## 1. Introduction

Eutrophication and harmful algal blooms are increasingly common in aquatic ecosystems worldwide (Heisler et al., 2008; Smith et al., 2006). Harmful algal blooms are typically triggered by excess inputs of the normally limiting nutrients nitrogen (N) and phosphorus (P) (Paerl, 2008), and are considered the greatest inland water quality threat to public health and environmental risk (Brooks et al., 2016; Gobler et al., 2012). Numerous works have addressed the spatio-temporal variation of nutrient and phytoplankton and chlorophyll-*a* (Chl-*a*) in freshwater ecosystems (such as reservoirs and lakes) and have highlighted the close relationship between riverine nutrient loading and phytoplankton biomass in reservoirs or lakes through measurement and modelling approaches (Kane et al., 2014; Mamun and An, 2017; Mo et al., 2016; Reartes et al., 2016). Internal nutrient release via diffusion and sediment resuspension may also contribute to algal blooms (Pearce et al., 2017; Søndergaard et al., 2003). Phytoplankton dynamics are site-specific and might be controlled by hydrological conditions and abiotic and biotic variables (Kuo and Wu, 2016). Understanding the nutrient cycling processes and key factors controlling phytoplankton succession and undesired algal bloom at various time scales is essential to develop site-specific strategies to mitigate eutrophication of aquatic ecosystems.

Climate change is predicted to have many diverse effects on lake and reservoir water quality and ecosystem functioning worldwide, due to changes in watershed hydrology and nutrient loading, water temperature, mixing regime, internal nutrient dynamics, and other factors (Paerl et al., 2016; Sin and Jeong, 2015; Wang et al., 2015). For example, rainfall-induced nutrient fluctuations in surface water affect phytoplankton communities and cause cyanobacteria blooms that are likely to occur in wet years (Qiu et al., 2016). Hydrochemistry and trophic state have changed in a large reservoir in the Brazilian northeast region under intense drought conditions (Santos et al., 2016). Enhanced stratification will influence nutrient availability and phytoplankton functional groups in deep reservoirs (Becker et al., 2009). However, most research on the effects of environmental change in freshwaters has focused on incremental changes in average conditions, rather than fluctuations caused by extreme events such as floods which need to be addressed to develop more accurate and predictive bio-assessments of the effects of fluctuations (Tweedley et al., 2016; Voynova et al., 2015; Woodward et al., 2016). Climate change is likely to increase tropical/subtropical cyclones and accompanying heavy storms, especially in subtropical East Asia (Webster et al., 2005; Wu et al., 2005). To date, the nutrient and phytoplankton dynamics in response to pulse inputs from storm runoff and key drivers controlling the formation of algal blooms are less documented.

Our previous research in southeast China has characterized the effect of major storms on the fluxes and processes related to nutrients being brought from the North Jiulong River catchment towards the estuary (Chen et al., 2012; Chen et al., 2015). We hypothesized that a reservoir ecosystem will be sensitive to pulse input of particulate matter and nutrient availability via storm runoff. Such storms were expected to increase the bioavailable nutrient forms (nitrate, ammonium, phosphate and organic nutrients) across the catchment but to different extents, depending on source supply and their transport paths (surface/subsurface runoff, and in-stream mobilization). Here we used opportunistic observational studies on the storm-driven runoff in a small dam reservoir (Xipi) in the middle North Jiulong River. We carried out high-frequency sonde measurement, daily sampling at the surface, and three-day sampling of the water column before, during and after storms that occurred in June–July 2015. The main questions we seek to address here are how storms change hydrochemistry and processes driving phytoplankton (Chl-*a*) variability. The specific objectives of this study were 1) to explore reservoir nutrient dynamics and nutrient-phytoplankton coupling in response to storm runoff, and 2) to determine the major factors controlling Chl-*a* evolution and algal bloom.

## 2. Materials and methods

### 2.1. Study area

The Jiulong River is a subtropical river located in southeastern China (Fig. 1), with a drainage area of 14,741 $km^2$. There are two main tributaries, the North River and West River. The watershed is under the Asian monsoon climate, subject to strongly seasonal variation of precipitation and temperature. The recorded mean annual air temperature is 20.9 °C, and annual precipitation is 1400–1800 mm, 75% of which occurs between May and October. Six major dams have been constructed along the main stem of the North River. Land use in the North River watershed includes 70% forest and upland orchards, 18% arable land and 5% urban and residential land. Pig farming in the upper stream area (Longyan city) has increased markedly since the late 1990s (Chen et al., 2013). The other counties (Zhangping, Hua'an) are predominantly agricultural and forest land and have a relatively low population intensity.

Xipi Reservoir is one of several cascade dam reservoirs located in the middle of the North River (Fig. 1). It began impounding water in 2008 for the purpose of hydropower generation and flood control, and now has a channel length of 8.5 km and mean width of 125 m. The same reservoir has previously been studied from perspectives of N and P cycling (Chen et al., 2014a; Lu et al., 2016; Zhou et al., 2016) and seasonal nutrient-phytoplankton dynamics (Mo et al., 2016). This study focuses on the effects of storm runoff on nutrient and phytoplankton in the lacustrine zone (0–2.5 km upstream of Xipi Dam). The main body of the reservoir has an open water area of 0.34 $km^2$, mean and maximum depth of 15 m and 28 m, a capacity of $389 \times 10^4$ $m^3$, and a relatively short HRT of less than a day (typical for a "run-of-the-river" reservoir). For a more detailed description of the study site see Mo et al. (2016). The dam is partly or completely opened during storm periods for flood controls depending on water level.

### 2.2. Sampling campaign and lab analysis

To capture nutrient and phytoplankton dynamics in reservoir water in response to storm runoff, daily measurements were conducted from June 18 through July 15, 2015 at site X3 in the lacustrine zone (Fig. 1). Surface (0.5 m) water was collected, filtered and stored in polyethylene bottles at a local house. The final sample collected on July 15 was excluded due to failure in sample storage. Vertical water samples were collected every three days at 1 m depth intervals using a SL-2A handheld electric deep water sampler (DEWALT® DC 740). A calibrated YSI sondes (6600, USA) was deployed at site X3 (1 m below water surface) to obtain hourly water temperature, pH, DO, turbidity, and chlorophyll. The YSI sondes was also used to measure the profile of the water column in three-day sampling.

All samples were filtered through a Waterman GF/F membrane, and frozen (−20 °C) until analysis. Nutrient forms analyzed included nitrate ($NO_3$–N), nitrite ($NO_2$–N), ammonium ($NH_4$–N), dissolved reactive phosphorus (DRP), dissolved total nitrogen (TDN) and phosphorus (TDP), and total particulate phosphorus (TPP) with total suspended matter (TSM). $NO_3$–N, $NO_2$–N, $NH_4$–N and DRP were analyzed by segmented flow automated colorimetry (San ++ analyzers, the Netherlands), using standard procedures and methods (Rice et al., 2005). DIN was defined as the sum of $NO_3$–N, $NO_2$–N and $NH_4$–N. TDN and TDP were determined as $NO_3$–N and DRP following oxidization with 4% alkaline potassium persulfate. Dissolved organic P (DOP) was obtained by subtracting DRP from TDP, and dissolved organic N (DON) was obtained by subtracting DIN from TDN. The pre-weighed and filtered GF/F membranes were oven-dried (105 °C) to constant weight, and concentrations of TSM were determined gravimetrically. The oven-dried membranes were analyzed for TPP after being combusted in a muffle furnace (550 °C for 1.5 h) and extracted with HCl. The precision for nutrient analysis was estimated by repeated determinations of 10% of the

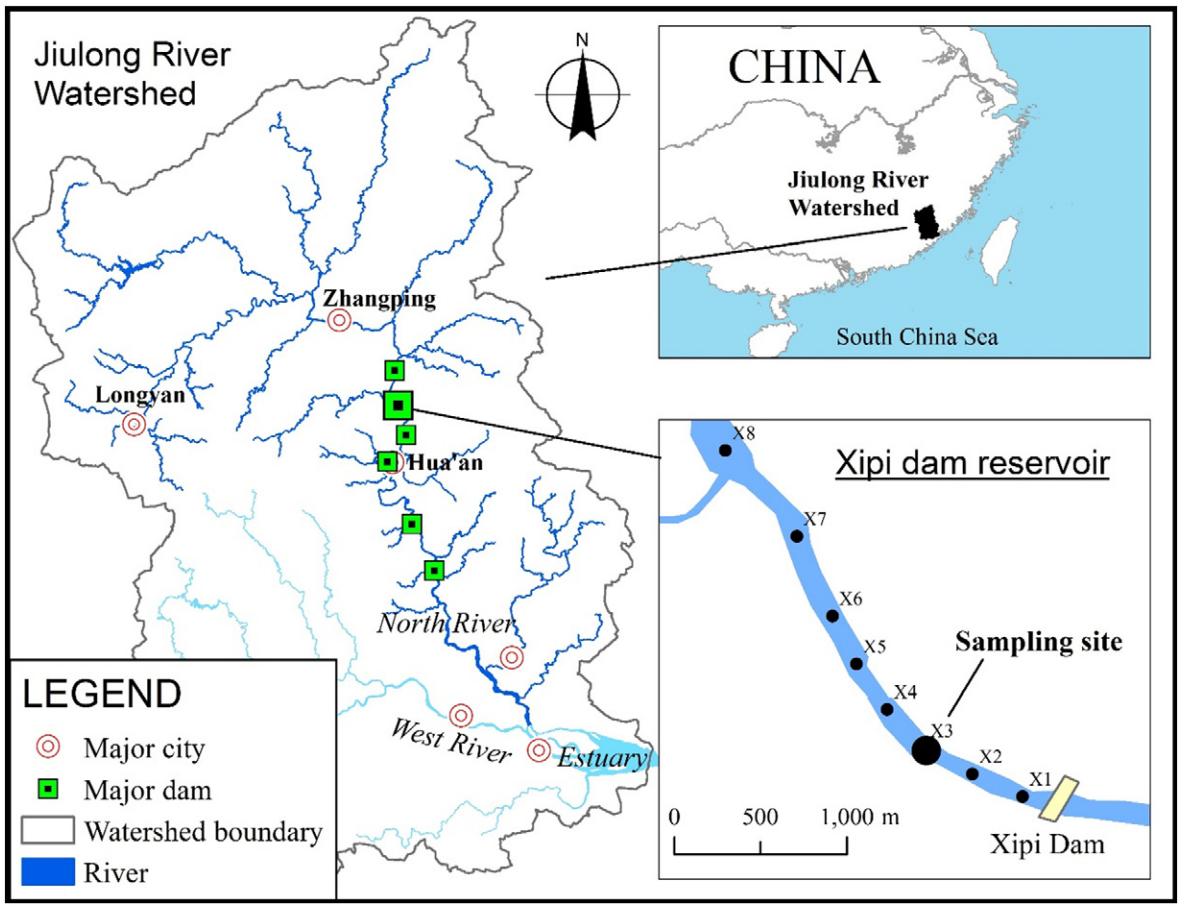


**Fig. 1.** Map of studied reservoir showing sampling site (X3) during storms.

samples and the relative error was 2%–5%. Commercial standard reference materials were used to check instrument performance.

Another set of sub water samples were filtered through 25 mm GF/F membranes for measurements of Chl-*a*. The filters were extracted with 90% acetone, and Chl-*a* was measured with a Turner fluorescence spectrophotometer (Parsons et al., 1984). A small amount of the surface (0.5 m) water sample was preserved in 4% formalin before identification of phytoplankton species using a microscope (400× or 1000× magnification; Nikon 90i). Other one liter surface samples were gathered with an organic-glass bottle and immediately preserved with 1% Lugol's iodine solution. The samples were settled for 48 h and then concentrated to 30 mL (Rice et al., 2005). After mixing, 0.1 mL of the concentrated sample was placed onto a 0.1 mL counting chamber (20 mm × 20 mm) and enumerated with an optical microscope (400× magnification). We counted cell number in triplicate and at least 300 cells per sample were counted to reduce uncertainty. Phytoplanktons were identified into seven categories according to algae characteristics, whether cells have chromosomes and nuclei or siliceous cell shell: Dinophyta, Bacillariophyta, Cyanophyta, Chlorophyta, Euglenophyta, Cryptophyta and others. The phytoplankton abundance (cell $L^{-1}$) was calculated by Eq. (1) (Casamayor et al., 2000).

$$N = \frac{S}{S_0} \times \frac{V_0}{V} \times n \quad (1)$$

where $N$ is phytoplankton abundance per liter water sample (cell $L^{-1}$). $S$ and $V$ refer to the counting chamber area ($mm^2$) and volume (0.1 mL), respectively. $S_0$ represents the counting area ($mm^2$), $V_0$ represents water sample volume (30 mL), and $n$ is the number of phytoplankton within the counting area (cells). Phytoplankton geometric shapes were measured to obtain the approximate cell volume. The phytoplankton biomass (wet weight) was estimated assuming a wet weight density of 1 g $cm^{-3}$ (Wetzel and Likens, 2000).

### 2.3. Auxiliary data collection and data analysis

Hourly rainfall and air temperature at three weather stations (Longyan, Zhangping, and Hua'an) were derived from a Chinese weather website (http://www.weather.com.cn/); the hourly discharge (dam outflow) on the sampling date was obtained from Xipi hydropower dam office. Statistical analysis (regression, Pearson correlation, comparison with independent-samples *t*-test) with significance level at 0.05 was performed using SPSS 17.0. Surfer 12.0 was used for interpolation of three-day vertical measurements and daily surface measurements to the whole water column over time.

### 2.4. Dynamic factor analysis

Dynamic factor analysis (DFA) is a dimension-reduction technique that has been widely applied in aquatic ecosystem studies (Erzini, 2005; Kuo and Wu, 2016; Laine et al., 2007). We used DFA to explore the relationship between time-series data for explanatory and response variables at one day intervals. Unlike factor analysis and principal component analysis, DFA takes into account the time series component of the data which can be expressed as Eq. (2). The mathematical form of the DFA model is shown in Eqs. (3) and (4).

$$\begin{aligned} N \text{ response variables} = {} & \text{linear combination of } M \text{ common trends} \\ & + \text{explanatory variables} + \text{constant level parameter} \\ & + \text{error component} \end{aligned} \quad (2)$$

$$S_n(t) = \sum_{m=1}^{M} \gamma_{m,n}\alpha_m(t) + \mu_n + \sum_{k=1}^{K} \beta_{k,n}\upsilon_k(t) + \varepsilon_n(t) \quad (3)$$

$$\alpha_m(t) = \alpha_m(t-1) + \eta_m(t) \quad (4)$$

Response variable $S$ is Chl-*a* in this study. The common trends ($\alpha_m(t)$) represent one or more latent unknown patterns, which represent the non-explanatory variables in the time series. $\eta_m(t)$ is the noise component. The regression coefficients ($\beta_{k,n}$), weighting coefficients for the explanatory variables ($v_k(t)$), were used to determine whether the explanatory variable is significantly related to the response variable ($t$ value >2). $M$ and $K$ are numbers of common trend and explanatory variable, respectively. The constant level parameter ($\mu_n$) is the intercept term for shifting up or down each linear combination of common trends, and the error component ($\varepsilon_n(t)$) is assumed to be independent of each other, Gaussian-distributed with zero mean and unknown diagonal or non-diagonal covariance matrix.

Canonical correlation coefficients ($\rho_{m,n}$) quantify cross-correlation between response variables and common trend. The terms "high", "moderate", "low", and "weak" refer to the absolute values of canonical correlation coefficients >0.75, 0.50–0.75, 0.25–0.50 and <0.25, respectively. The Nash-Sutcliffe coefficient $C_{eff}$ (Nash and Sutcliffe, 1970) and Akaike's information criterion (AIC) (Akaike, 1974) were used to select the optimal-performing DFA model. DFA was performed using the statistical software package Brodgar Version 2.7.4 (Highland Statistics Ltd., Newburgh, UK). A complete and detailed description of DFA can be found in Zuur et al. (2003).

Four scenarios (configurations of the important explanatory variables) were considered in the DFA models to investigate the key factors controlling Chl-*a* variations. Model I considered all monitoring variables as possible explanatory variables while Model II considered a one-step time-delay of all monitoring variables. Model III excluded TDN, DIN, DON, DTP, TPP, and DOP as explanatory variables due to a degree of overlap with other nutrient forms (e.g., DIN = $NO_3$–N + $NO_2$–N + $NH_4$–N) and data availability from the current auto-monitoring program in China (e.g., TPP, DON, DOP was not applicable). Model IV considered a one-step time-delay of the explanatory variables in Model III. Time series data from June 18 through July 11, 2015 were used in the models to simulate the complete cycle of first peak Chl-*a*.

## 3. Results

### 3.1. Characteristics of storm events and hydrology

A heavy rain storm occurred on June 20, 2015, concentrated on Hua'an (study site). A second rain storm in early July at first concentrated on Longyan then expanded downward to Zhangping and Hua'an. The mean precipitation recorded at three weather stations in the upper river watershed was 43.8 mm. Another storm caused by Typhoon Chanhom occurred on July 5 with a peak precipitation of 70.4 mm in Zhangping (close to study site); this storm lasted 98 h and produced a total mean precipitation of 55.6 mm. Daily water discharge at the dam bottom outflow increased to a peak value of 254 $m^3\ s^{-1}$ on June 21, well above summer "normal" hydrological conditions (~100 $m^3\ s^{-1}$) (Fig. 2a). As the second rainfall mainly occurred in the upper area, discharge in early July was not nearly as high as discharge during the first rain event. There were also some minor rainfall events (accumulated rainfall 5.1–39.2 mm) on June 11–14 (data not shown), a few days before we began sampling on June 18, 2015. These earlier rain events prior to sampling may impact the starting conditions of the study period. For example, discharge was already very high at the very start of the study period, likely due to these prior minor rainfall events.

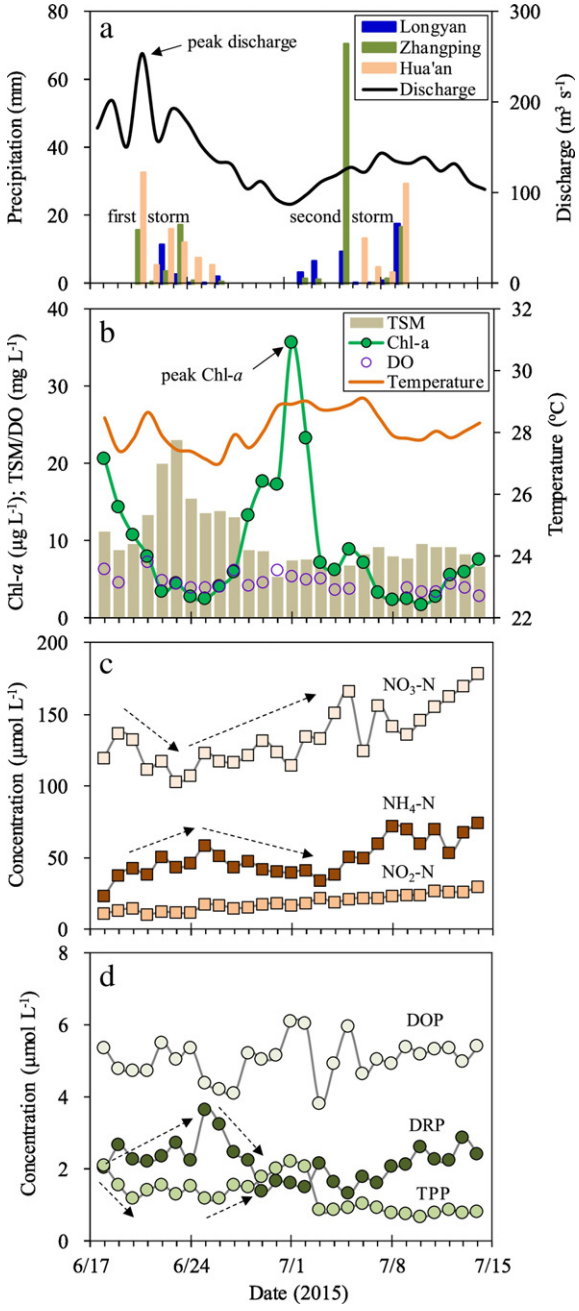


**Fig. 2.** Daily variation of rainfall at weather stations and discharge of dam outflow (a), physiochemical parameters (TSM, water temperature and DO) (b), nitrogen (c) and phosphorus (d). Dashed arrows indicate the temporal trend of nutrients following first storm.

### 3.2. Temporal variation of physiochemical parameters and nutrients under storms

Driven by precipitation and somewhat regulated by dam operation, a temporal variation of discharge (74–254 $m^3\ s^{-1}$), water temperature (27.0–29.1 °C), DO (3.4–7.2 mg $L^{-1}$), pH (6.7–7.4), TSM (5.3–23.0 mg $L^{-1}$) and Chl-*a* (1.7–35.6 μg $L^{-1}$) were observed (Fig. 2a–b). TSM increased sharply with discharge and its maximum value was observed two days after peak discharge. Thereafter, TSM returned to base flow level (<10 mg $L^{-1}$) and was elevated slightly in the second rain storm. In contrast, Chl-*a* declined dramatically at first before increasing gradually to a peak value (35.6 μg $L^{-1}$) 10 days after peak discharge. When the second rain storm occurred, Chl-*a* dropped again to <5 μg $L^{-1}$ before recovering slightly by end of sampling.

Nutrient concentrations varied with changing discharge (Fig. 2). $NO_3$-N (103–178 μmol $L^{-1}$) dropped when the first rain storm occurred on June 20 (a similar phenomenon was observed during the second storm on July 5), then elevated gradually in the falling hydrograph limb. In contrast, the increase in $NH_4$-N (22.8–74.1 μmol $L^{-1}$) appeared to have started before the first rain storm event and continued to increase following the two storms. Subsequently it declined when the first rain storm stopped, before increasing again and appearing to be steady towards the end of sampling. $NO_2$-N (10.2–29.9 μmol $L^{-1}$) increased gradually during the sampling period. DRP (1.3–3.6 μmol $L^{-1}$) appeared to be similar to $NH_4$-N behavior, as both peaked on June 25, 3 days after the storm event and started to increase on July 5 following the second rain storm. TPP changed little around peak discharge, but increased in the falling limb of the hydrograph before a sharp decline with increasing discharge caused by the second storm. DOP (3.8–6.1 μmol $L^{-1}$) exhibited a greater fluctuation than other nutrient forms.

Nutrient composition changed as well (Fig. 3). DIN was dominated by nitrate (73%–78%) prior to the storm. The fraction of $NO_3$-N to DIN decreased with rising discharge (62%–70%) before increasing in the falling hydrograph limb (66%–71%). $NH_4$-N fraction was as low as 15% prior to the storm but increased to 23%–29% in the flooding periods, while the $NO_2$-N fraction was small and variable (6%–11%). DOP was the dominant P form (53%–59% of TP), decreasing to 48% four days after peak discharge, and thereafter increasing to a higher fraction (>60%). The DRP fraction varied widely (16%–40%), increasing from about 26% prior to the storm to up to 40% four days after peak discharge, before decreasing and then increasing again in the second storm (24%–33%). The TPP fraction decreased from 22% to 13% before peak discharge but increased back to 17%–23% with high Chl-*a*; thereafter, the TPP fraction was lower (8%–13%).

The correlations between measured parameters are detailed in Table 1. TSM was positively correlated with discharge ($p < 0.01$). Major nutrients ($NO_3$-N, $NO_2$-N, $NH_4$-N) were positively correlated with conductivity while TSM was negatively correlated with conductivity ($p < 0.01$). Correlation of P forms was not as good as N, with the exception of DRP which was correlated with temperature and TSM ($p < 0.05$). DSi

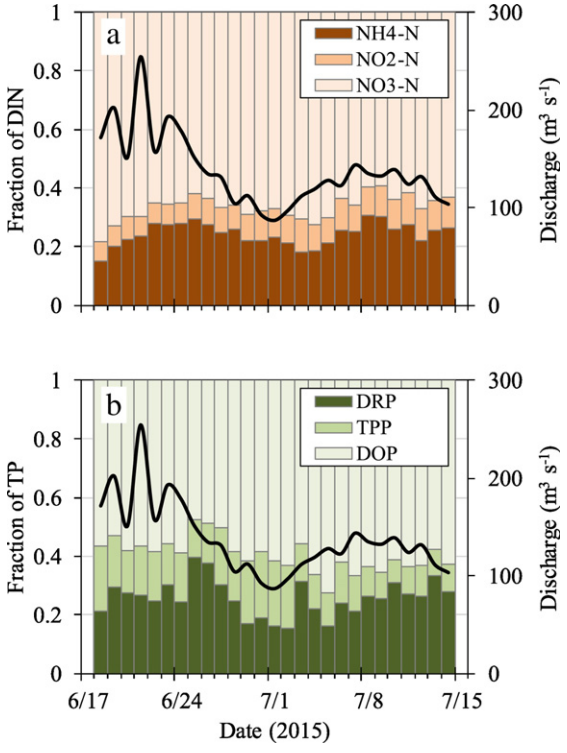


**Fig. 3.** Daily variation in (a) nitrogen, and (b) phosphorus compositions. Curved line indicates discharge of dam outflow.

**Table 1**
Pearson correlation coefficients of each parameter of surface water under storms.

| | Discharge | Precipitation | Temperature | DO | Conductivity | TSM | $NO_2$-N | $NO_3$-N | $NH_4$-N | DON | DRP | DOP | TPP | DSi | Chl-*a* |
|---|---|---|---|---|---|---|---|---|---|---|---|---|---|---|---|
| Discharge | 1 | | | | | | | | | | | | | | |
| Precipitation | 0.245 | 1 | | | | | | | | | | | | | |
| Temperature | −0.327 | −0.176 | 1 | | | | | | | | | | | | |
| DO | 0.324 | −0.075 | 0.372 | 1 | | | | | | | | | | | |
| Conductivity | −0.476* | −0.289 | 0.108 | −0.608** | 1 | | | | | | | | | | |
| TSM | 0.599** | 0.263 | −0.524** | 0.115 | −0.514** | 1 | | | | | | | | | |
| $NO_2$-N | −0.583** | −0.164 | 0.184 | −0.608** | 0.791** | −0.589** | 1 | | | | | | | | |
| $NO_3$-N | −0.380 | −0.232 | 0.211 | −0.567** | 0.799** | −0.590** | 0.832** | 1 | | | | | | | |
| $NH_4$-N | −0.240 | 0.124 | −0.262 | −0.705** | 0.637** | −0.138 | 0.749** | 0.571** | 1 | | | | | | |
| DON | −0.399* | −0.136 | −0.215 | −0.079 | −0.219 | −0.009 | 0.034 | −0.321 | 0.074 | 1 | | | | | |
| DRP | 0.331 | 0.064 | −0.773** | −0.217 | −0.131 | 0.489** | −0.066 | −0.149 | 0.266 | 0.222 | 1 | | | | |
| DOP | −0.220 | −0.029 | 0.300 | −0.183 | 0.390* | −0.155 | 0.115 | 0.222 | 0.116 | −0.260 | −0.495** | 1 | | | |
| TPP | 0.019 | −0.154 | 0.178 | 0.661** | −0.466* | 0.140 | −0.682** | −0.624** | −0.693** | 0.183 | −0.262 | 0.270 | 1 | | |
| DSi | −0.261 | −0.516** | 0.286 | 0.025 | 0.229 | −0.323 | 0.317 | 0.343 | −0.001 | 0.163 | −0.065 | 0.194 | 0.049 | 1 | |
| Chl-*a* | −0.302 | −0.246 | 0.457* | 0.439* | −0.103 | −0.336 | −0.279 | −0.217 | −0.553** | 0.109 | −0.470* | 0.433* | 0.791** | 0.241 | 1 |

Note: significance level, * $p < 0.05$; ** $p < 0.01$. Sample number = 27.

was negatively correlated with precipitation ($p < 0.05$). In addition, Chl-*a* was positively correlated with temperature, DOP, and TPP while negatively correlated with $NH_4$-N and DRP ($p < 0.05$).

### 3.3. Change in Chl-a and phytoplankton under storms

High-frequency measurement using YSI sondes captured real-time changes in physiochemical parameters and Chl-*a* (Fig. 4). Turbidity exhibited the same temporal pattern as TSM (Fig. 2) and a good linear regression exists between turbidity (Y) and TSM (X) ($Y = 2.12X - 8.58$, $R^2 = 0.92$, $p < 0.01$). In general, sensor monitored Chl-*a* had a similar trend with in-lab measurements.

As another indicator of biomass, phytoplankton abundance ($4.63 \times 10^5$–$1.16 \times 10^7$ cell $L^{-1}$) followed the same temporal pattern as Chl-*a* (Fig. 5a). The major phytoplankton groups ordered by percentage were: Chlorophyta (7%–82%), Cyanophyta (4%–69%), Bacillariophyta (2%–35%) and Dinophyta (1%–19%). Cryptomonas, Euglenophyta and others contributed 2%–8% of total phytoplankton abundance. A higher Cyanophyta fraction was found during and after algal bloom (peak Chl-*a*) though Chlorophyta was still the dominant phytoplankton group, accompanied with an increasing DIN:DRP ratio (Fig. 5b). Enrichment of nitrate and ammonium following storms therefore resulted in an elevation of the DIN:DRP ratios.

Correlation analysis showed that Cyanophyta was positively correlated with temperature ($p < 0.05$) while negatively correlated with TSM ($p < 0.05$) (Table 2). Only Dinophyta was correlated with discharge ($p < 0.05$). Most of phytoplankton except Bacillariophyta and Cyanophyta was negatively correlated with $NH_4$-N ($p < 0.05$). There are four groups were negatively correlated with DRP ($p < 0.05$). In contrast, most phytoplankton groups were positively correlated with TPP and Chl-*a* ($p < 0.01$). Only Bacillariophyta and Cyanophyta were positively correlated with DOP ($p < 0.05$), and Bacillariophyta, Cyanophyta, Chlorophyta, and Euglenophyta were positively correlated with DO ($p < 0.05$). In particular, the proportion of Cyanophyta to total abundance (%) was positively correlated with inorganic N ($NO_3$-N, $NO_2$-N, $NH_4$-N) while negatively correlated with TPP ($p < 0.05$). The Chlorophyta proportion and Chl-*a* were significantly correlated ($p < 0.05$) (Table 2).

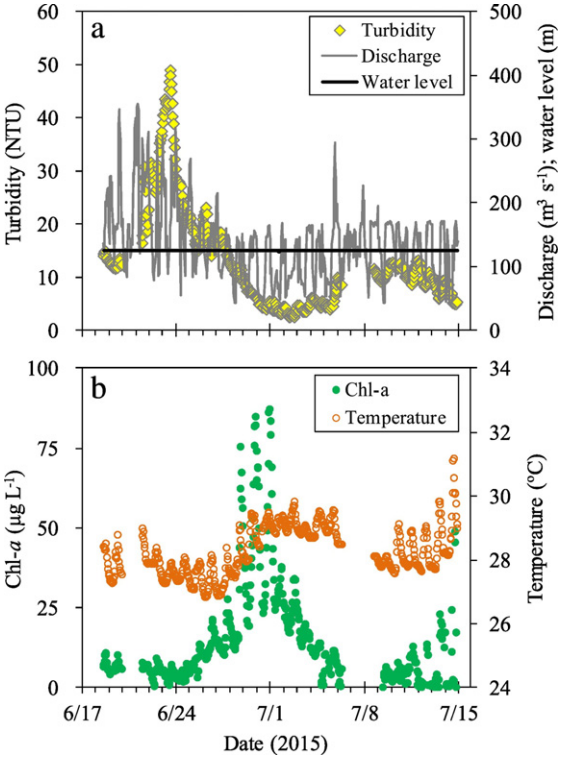


**Fig. 4.** High-frequency (hourly) measurement of turbidity and discharge (a), Chl-*a* and temperature (b) using a YSI sondes deployed in lacustrine zone (site X3) during storm events. Some data points were missing due to equipment maintenance. Hourly discharge of dam outflow and water level (124.7–125.8 m) are also shown in the top panel.

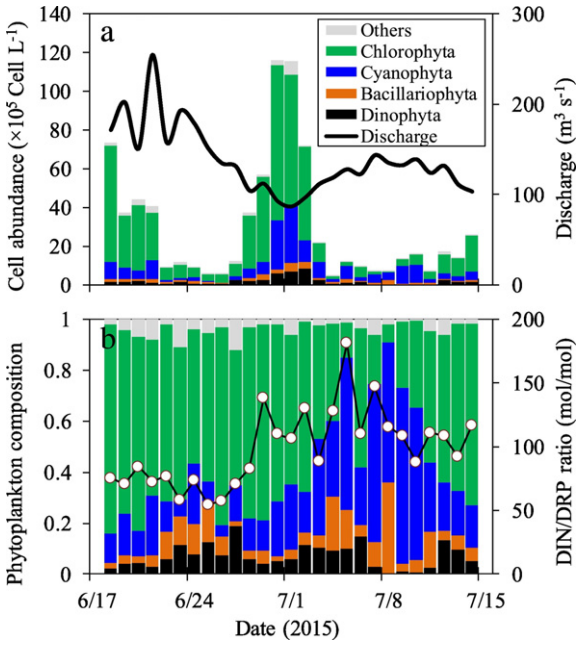


**Fig. 5.** Daily variations of phytoplankton abundance (a) and community composition (b). Blank circles in the bottom panel indicate molar DIN:DRP ratio.

### 3.4. Thermal stratification and vertical distribution of nutrients and Chl-a

Thermal stratification existed with a temperature difference of 2 °C across the water column prior to the storm as well as other low discharge periods (Fig. 6a). Conductivity decreased with water depth (142–193 μS $cm^{-1}$) but increased markedly following storms (Fig. 6b). TSM overall increased with water depth (9.6–20.2 mg $L^{-1}$) (Fig. 6c). DO was higher in surface water than bottom water (4.9–6.4 mg $L^{-1}$) (Fig. 6d). During flooding periods, stratification was weakened with minor temperature differences and most parameters were distributed almost evenly in the water column (Fig. 6). Chl-*a* maximum was usually found at a water depth of 0.5–2 m but disappeared in high discharge periods (Fig. 6g).

The $NH_4$-N concentration in the water column was elevated following the first storm while an apparent removal in surface water was observed, accompanied with high Chl-*a* (17.3 μg $L^{-1}$), on June 30, 2015. In this case, average Chl-*a* (10.8–17.3 μg $L^{-1}$) in the upper layer (0.5–1 m) was significantly greater than in the deep layer (2–16 m) (0.9–5.8 μg $L^{-1}$). In contrast, $NH_4$-N concentrations in the upper layer (40–43 μmol $L^{-1}$) were about 10% lower than in the deep layer (42–50 μmol $L^{-1}$), and DRP in the upper layer (1.7 μmol $L^{-1}$) was 25% lower than in the deep layer (1.8–2.6 μmol $L^{-1}$). TPP was higher in the upper layer (1.4–2.0 μmol $L^{-1}$) than in the deep layer (0.9–1.2 μmol $L^{-1}$). The average concentration difference (Δ) between upper and deep layers was calculated as $\Delta$Chl-*a* = 11.6 μg $L^{-1}$, $\Delta NH_4$-*N* = −5 μmol $L^{-1}$, $\Delta$DRP = −0.5 μmol $L^{-1}$, and $\Delta$TPP = 0.6 μmol $L^{-1}$. In contrast, maximum $NO_3$-N (133 μg $L^{-1}$) and $NO_2$-N (20 μg $L^{-1}$) was found at a depth of 4 m. $NO_3$-N in the surface layer (124–128 μmol $L^{-1}$) was far greater than in bottom water (16 m) (109 μg $L^{-1}$).

### 3.5. DFA results

The optimal-performing DFA models for describing Chl-*a* variations were developed for four scenarios in terms of the explanatory variables configuration (Table 3). Various combinations of explanatory variables

**Table 2**
Pearson correlation coefficients between phytoplankton and chemical parameters under storms.

| | Discharge | Temperature | DO | Conductivity | TSM | $NO_2$-N | $NO_3$-N | $NH_4$-N | DRP | DOP | TPP | DSi | Chl-*a* |
|---|---|---|---|---|---|---|---|---|---|---|---|---|---|
| Abundance (cells $L^{-1}$) | | | | | | | | | | | | | |
| Dinophyta | −0.432* | 0.445* | 0.272 | −0.015 | −0.301 | −0.137 | −0.197 | −0.426* | −0.413* | 0.367 | 0.708** | 0.077 | 0.825** |
| Bacillariophyta | −0.253 | 0.441* | 0.579** | 0.127 | −0.251 | −0.159 | −0.141 | −0.271 | −0.514** | 0.542** | 0.606** | 0.058 | 0.800** |
| Cyanophyta | −0.310 | 0.424* | 0.411* | 0.123 | −0.431* | −0.052 | −0.157 | −0.300 | −0.460* | 0.408* | 0.540** | 0.070 | 0.756** |
| Chlorophyta | −0.215 | 0.355 | 0.435* | −0.143 | −0.292 | −0.313 | −0.277 | −0.541** | −0.381* | 0.330 | 0.811** | 0.246 | 0.881** |
| Euglenophyta | −0.212 | 0.294 | 0.406* | −0.174 | −0.208 | −0.335 | −0.382* | −0.468* | −0.328 | 0.235 | 0.745** | 0.156 | 0.831** |
| Cryptomonas | 0.135 | 0.160 | 0.206 | −0.189 | −0.026 | −0.367 | −0.342 | −0.382* | −0.143 | 0.175 | 0.485* | −0.108 | 0.642** |
| Others | −0.432* | 0.445* | 0.272 | −0.015 | −0.301 | −0.137 | −0.197 | −0.426* | −0.413* | 0.367 | 0.708** | 0.077 | 0.825** |
| Composition (%) | | | | | | | | | | | | | |
| Dinophyta | −0.166 | −0.074 | −0.433* | −0.262 | 0.194 | −0.054 | −0.111 | −0.199 | 0.140 | −0.280 | 0.052 | 0.007 | −0.059 |
| Bacillariophyta | 0.035 | −0.088 | 0.058 | 0.245 | 0.079 | 0.147 | 0.164 | 0.366 | −0.001 | 0.015 | −0.377 | −0.077 | −0.392* |
| Cyanophyta | −0.104 | 0.108 | 0.100 | 0.496** | −0.399* | 0.460* | 0.399* | 0.401* | −0.374 | 0.201 | −0.508** | −0.164 | −0.273 |
| Chlorophyta | 0.059 | 0.006 | 0.025 | −0.430* | 0.220 | −0.406* | −0.341 | −0.427* | 0.276 | −0.077 | 0.573** | 0.221 | 0.418* |
| Euglenophyta | 0.015 | −0.250 | −0.092 | −0.326 | 0.235 | −0.288 | −0.351 | −0.139 | 0.192 | −0.380 | 0.262 | −0.090 | 0.026 |
| Cryptomonas | 0.495** | −0.300 | −0.170 | −0.352 | 0.450* | −0.408* | −0.357 | −0.238 | 0.175 | −0.222 | 0.149 | −0.331 | 0.026 |
| Others | 0.148 | −0.424* | −0.537** | −0.110 | 0.463* | −0.005 | −0.197 | 0.099 | 0.320 | −0.286 | −0.264 | −0.043 | −0.485* |

Note: significant level, * $p < 0.05$; ** $p < 0.01$. Sample number = 27.

were considered in each scenario and then the optimal DFA model was determined based on AIC and $C_{eff}$ values. All four models produced reasonable simulated results compared with observed Chl-*a* ($C_{eff}$ values = 0.87–0.89). Model I showed that water temperature, TSM and TPP were significantly correlated with Chl-*a* ($t > 2$). In Model II (which includes a one-step time-delay of all monitoring variables), temperature, TSM and TPP were again correlated with Chl-*a*. In Model III (which excludes the explanatory variables TDN, DIN, DON, DTP, TPP and DOP), pH, TSM, $NO_3$-N and $NH_4$-N were significantly correlated with Chl-*a*. In Model IV (which considers a one-step time-delay of the explanatory variables in Model III), discharge, TSM, $NH_4$-N and DRP were negatively correlated while TP was positively correlated with Chl-*a*. Based on these DFA models, simulated values versus observed values are shown in Fig. 7. Model II had the lowest AIC (31.3), while Model IV had the highest $C_{eff}$ (0.89) and adjusted $R^2$ (0.880), and exhibited the best performance in predicting Chl-*a* variation following the storm. Both Model II and IV indicate that a one-step time-delay of TSM negatively affect the variations of Chl-*a*. In addition, TPP in Model II and TP in Model IV had the highest contributions to Chl-*a* variation.

## 4. Discussion

### 4.1. Storm runoff driven nutrient dynamics in the river reservoir

River nutrient concentrations might change at different rates with transport from varying source areas by different flow pathways within the catchment (Chen et al., 2012; Chen et al., 2015). The large catchment area to reservoir area (CA:RA) ratio for Xipi reservoir meant that nutrient loading was dominated by watershed inputs via river transport. The concentrations of $NH_4$-N and DRP were elevated during high flow periods (Fig. 2), largely due to overland flushing via surface runoff. In general, $NH_4$-N is usually from wastewater and $NH_3$ fertilizers that survive from nitrification, and DRP mainly accumulates in the upper soil layer of croplands and waste water (Carpenter et al., 1998; Sims et al., 1998). Storm runoff may quickly carry $NH_4$-N and DRP that accumulated in the watershed to the river. A similar initial flushing effect has been widely recognized in previous studies (Bernal et al., 2012; Hathaway et al., 2012; Jones et al., 2008; Obermann et al., 2009; Tzoraki et al., 2007). $NH_4$-N increased further during and after the second rain storm, likely a result of

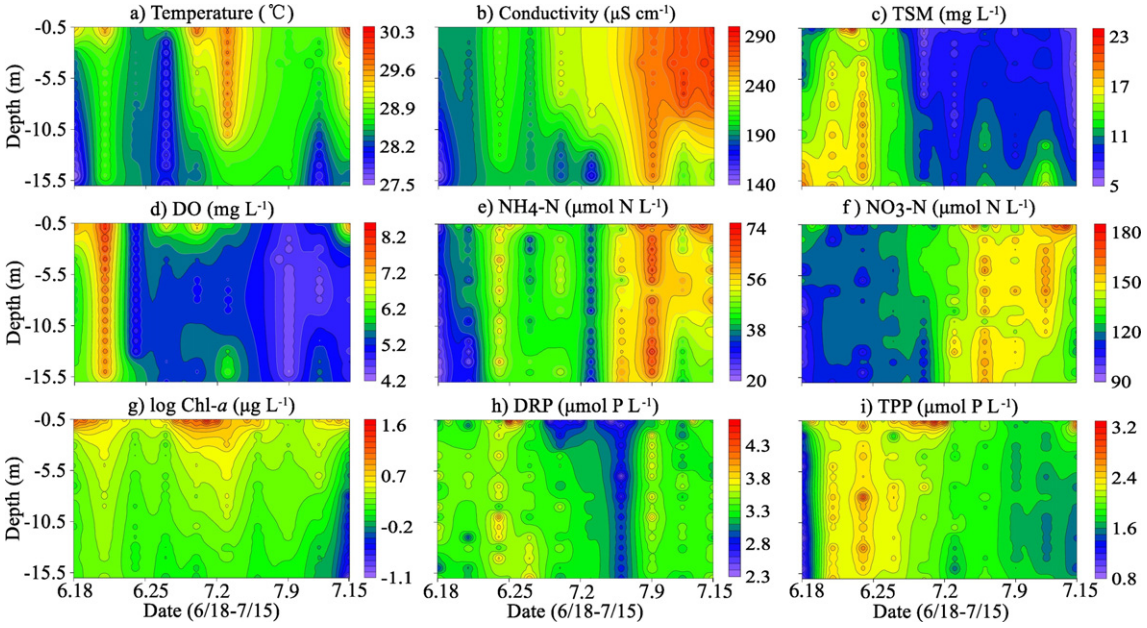


**Fig. 6.** Vertical distribution of physicochemical parameters, Chl-*a* and nutrients at Site X3. Surfer 12.0 was used for interpolation of three-day vertical measurements and daily surface measurements to the whole water column over time.

**Table 3**
A summary of DFA model results for Chl-*a* with four scenarios.

| Model styles | AIC | $C_{eff}$ | Adjusted $R^2$ | Explanation variables | | | | | | | | | | |
|---|---|---|---|---|---|---|---|---|---|---|---|---|---|---|
| | | | | Rainfall | Discharge | Temperature | pH | TSM | DTP | TPP | $NO_3$-N | $NH_4$-N | DRP | TP |
| Model I | 32.8 | 0.87 | 0.872 | 0.08 | – | **0.24*** | – | **−0.33*** | 0.09 | **0.80*** | – | – | – | – |
| Model II | 31.3 | 0.87 | 0.876 | – | −0.12 | **0.18*** | – | **−0.32*** | 0.06 | **0.88*** | – | – | – | – |
| Model III | 34.1 | 0.88 | 0.875 | 0.16 | – | – | **0.36*** | **−0.53*** | – | – | **−0.21*** | **−0.56*** | – | **0.43*** |
| Model IV | 33.0 | 0.89 | 0.880 | – | **−0.20*** | – | – | **−0.44*** | – | – | −0.19 | **−0.35*** | **−0.25*** | **0.60*** |

Note: Model I includes all monitoring variables, Model II considers a one-step time-delay of all monitoring variables, Model III removes TDN, DIN, DON, DTP, TPP, and DOP as explanatory variables, and Model IV considers a one-step time-delay of explanatory variables in Model III. * indicates significantly related to Chl-*a* (*t* value >2). The regression parameters determined to be significant using the *t*-test (*t* > 2) are shown in bold characters. AIC (Akaike's information criterion), the lowest number represents the optimal model; Coefficients of efficiency ($C_{eff}$) are computed with the combined set of predicted versus observed values for the response variables time series. Adjusted $R^2$ indicates regression of simulated and observed values as shown in Fig. 7.

flushing of waste water from the upper polluted area (Longyan and Zhangping) wherein rainfall was concentrated.

Unlike $NH_4$-N, the decline in nitrate levels at the start of the measurement period implies that within-channel mobilization can be diluted by rain water and surrounding runoff. The slower elevation of nitrate compared to $NH_4$-N (Fig. 2c) implies a delayed input. Nitrate concentration in the upper tributaries (Longyan) is as high as $NH_4$-N (Chen et al., 2014b). We argue that nitrate transport via surface runoff and within-channel mobilization is less likely to cause such a delayed increase in the reservoir. Previous studies suggest that soil may become oversaturated with nitrate and the elevated ground water table causes nitrate-rich ground water to re-discharge into the river channel (Molenat et al., 2002; Ocampo et al., 2006). In our previous work, we also observed the contrasting patterns between nitrate and ammonium behavior in the storm runoffs based on measurement at the river outlet (Jiangdong) during storms and baseflow survey in the river network (Chen et al., 2012). These results implied that a slower groundwater redisharge into the river might explain the delayed elevation of nitrate, although we did not measure it directly. The nitrate-discharge relationship varying with time and watersheds suggests the existence of complex hydrological mechanisms (Luz Rodriguez-Blanco et al., 2009; Wagner et al., 2008). Further studies investigating the relative importance of various transport pathways at the watershed scale are needed to fully understand nitrate and other nutrients delivery to the river-reservoir system.

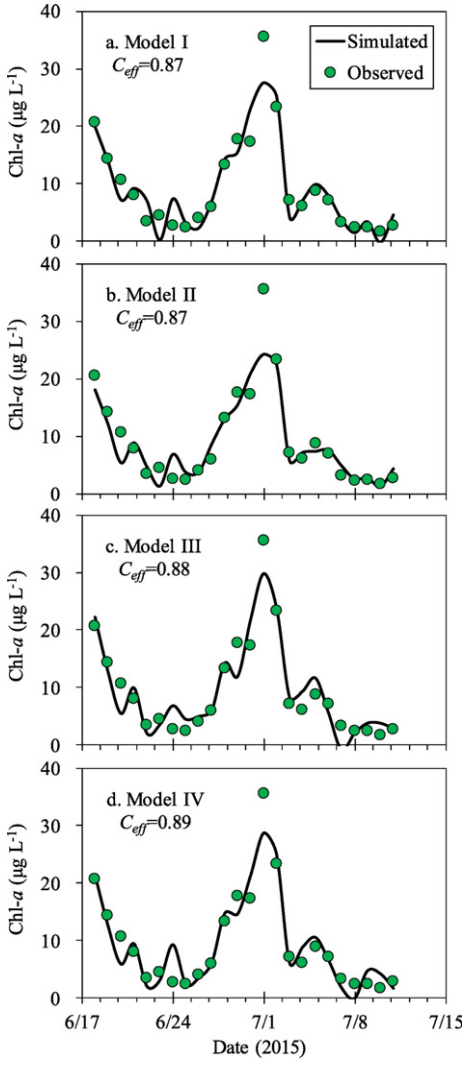


**Fig. 7.** Fitting curves of Chl-*a* in response to the storm runoff based on DFA with different parameterization. Coefficients of efficiency (Ceff) are computed with the combined set of predicted versus observed values for the response variables time series.

Storm runoff changes riverine nutrients but to different extents, depending on rainfall (size and distribution), antecedent soil moisture, and source supply (Chen et al., 2015; Chen et al., 2012). Watershed processes such as overland flushing via surface runoff, recharging to river channel via subsurface runoff or groundwater, or in-stream mobilization determined the nutrient dynamic in the river and reservoir. Storm runoff will cause a non-proportional change of nutrient forms. As a consequence, nutrient concentration, composition and N:P ratios varied with changing hydrography. In general, $NH_4$-N and DRP are relatively enriched compared with nitrate and DOP in storm runoff (Fig. 3).

TSM and turbidity increased quickly following the first storm (Fig. 2 and Fig. 4), suggesting that storm runoff around Hua'an and Zhangping accelerated the delivery of eroded sediment from the highlands. However, TSM and turbidity were relatively stable after the second storm since sediment carried by storm runoff (mainly occurring in the upper area) can be partly trapped behind other dam reservoirs. Previous studies have also observed similar responses to storm runoff (Chun et al., 2010; Correll et al., 1999), and a positive correlation between TSM and river discharge (Table 1, $p < 0.01$) further supported this conclusion. However, the temporal pattern exhibited by TPP differed from TSM (Fig. 2) and the correlation between them was not significant (Table 1). As a result, we speculated that particulate P in the river reservoir was only partly derived from eroded particles with other controls (see more discussion below). In fact, change in river TPP was associated with P attached in sediment (mineral particles) and organisms (algae, bacteria, and organic matter) (Hu et al., 2009).

### *4.2. Hydrochemical controls on phytoplankton in response to storm runoff*

High-frequency measurement and daily samples captured the temporal variation of physiochemical parameters, including chlorophyll *a* and phytoplankton taxa under storm conditions (Figs. 4–5). Chl-*a* and phytoplankton abundance decreased sharply when TSM or turbidity increased, largely due to the "shading" effect of high turbidity water and high flow turbulence that limited algal growth. During the studied periods, the dam sluices were partly open for power generation and flood controls; this resulted in large sub-daily variations in discharge, though the water level in the reservoir was relatively stable (124.7–125.8 m). Chl-*a* had a larger sub-daily variation than nutrients, likely a combined result of changing light availability and water turbulence (Fig. 4). Thereafter,

Chl-*a* and phytoplankton abundance elevated steadily, indicating that low turbidity (more light availability) and sufficient nutrient supply enhanced primary production. An algal bloom has been defined as Chl-*a* >30 or 40 μg $L^{-1}$ in lakes and reservoirs (Heiskary and Walker, 1995; James and Havens, 1996; Wu and Xu, 2011). In this study, Chl-*a* did exceed 30 μg $L^{-1}$ (Figs. 2 and 4) and an algal bloom dominated by Chlorophyta and Cyanophyta was apparently formed in the low discharge period (Fig. 5). A reduced discharge with stable water level adjusted by dam operation would have promoted the build-up of chlorophyll and phytoplankton.

Here we examined the nutrient-phytoplankton coupling processes following the storm events. In particular, once the turbidity and TSM was close to the lowest recorded level (June 30–July 2, 2015), TPP peaked while Chl-*a* concentration was highest (Fig. 2). The vertical distribution (higher TPP and lower DRP corresponding with higher Chl-*a* in the upper water layer compared to deep water) (Fig. 6), and their average concentration difference (ΔDRP = −0.5 μmol $L^{-1}$, near ΔTPP = 0.6 μmol $L^{-1}$) suggests that DRP had been consumed and integrated into phytoplankton biomass as organic P compounds. In an earlier study where measurements were conducted on a monthly basis, we also found that local algal sources contributed to the high TPP in the dry-wet transition period (Mo et al., 2016). Nitrogen is also a vital nutrient in photosynthesis. Our results show that $NH_4$-N had been removed together with DRP, while nitrate changed little during high Chl-*a* periods (Fig. 2).

Assuming photosynthesis followed the Redfield ratio (106C:16N:1P), the observed Δ$NH_4$-N: ΔDRP (=10) implies that phytoplankton during the bloom event preferentially used ammonium as an N source. Based on an enrichment experiment, Domingues et al. (2011) suggested that green algae and cyanobacteria preferred ammonium while diatoms preferred nitrate as an N-source. In this study, the pre-nutrient condition (relative enrichment of $NH_4$-N and DRP derived from storm runoff) might have favored proliferation of Chlorophyta and Cyanophyta, overwhelming other phytoplankton taxa (Fig. 5). Chlorophyta abundance was negatively correlated with $NH_4$-N ($p < 0.01$) (Table 2). In other words, $NH_4$-N and DRP were likely responsible for the observed algal bloom. In addition, Cyanobacteria generally grow better at higher temperatures (often above 25 °C) than do other phytoplankton species (Joehnk et al., 2008). Our data showed that Cyanophyta was positively correlated with temperature ($p < 0.05$) and elevated with increasing temperature.

DFA results further identified the determining factors controlling Chl-*a* evolution and algal bloom. A one day delay of discharge and TSM negatively affected the variations of Chl-*a* in Model IV. Chl-*a* variation was mainly controlled by turbidity, $NH_4$-N, DRP, TP and discharge (Table 3). In summary, low turbidity, sufficient nutrient supply and warming water are likely to trigger algal blooms following summer storms. Our DFA (Model IV) seems most suitable for early warning of algal blooms and we recommend Model IV (one-day delay of explanatory variables, lowest AIC and highest $C_{eff}$) as a practical tool to predict Chl-*a* variation. However, this model requires further verification in future, and we recommend adding DRP as an important parameter to the current auto-monitoring program as other parameters (discharge, $NH_4$-N, TP, turbidity, etc.) are available. High-frequency data will provide significant benefits to the understanding of the chemical and ecological status of aquatic systems. Furthermore, in order to mitigate eutrophication and reduce undesired algal blooms, watershed management actions should emphasize controlling dissolved nutrient loading, as discussed in our earlier work (Chen et al., 2013) and suggested by Wang et al. (2015).

## 5. Conclusions

The linkage between the mentioned parameters and hydrological conditions within the river reservoir were observed. A conceptual schematic of the nutrient-phytoplankton relationship as well as a very rapid response to storm runoff is illustrated in Fig. 8. Our high-frequency measurement and sampling during summer storm episodes successfully captured the physical-chemical parameter dynamics, particularly inorganic nutrients. $NH_4$-N and DRP were elevated during high flow periods due to overland flushing. Nitrate increased gradually after peak discharge likely due to a delayed input of groundwater. Correlation analysis and DFA Model suggested that Chl-*a* variation was mainly controlled by turbidity, $NH_4$-N, DRP, TP and discharge. Decreasing turbidity, sufficient nutrient supply and warming water in low flow periods are likely to trigger algal bloom, with a proliferation of Chlorophyta and Cyanophyta. Storm runoff was the main driver of nutrient delivery and cycling and phytoplankton succession (algal bloom) in the river-reservoir system. The reservoir ecosystem was vulnerable to pulse input of nutrient and particles from storm runoff and the Cyanophyta bloom was likely fueled by phosphate and ammonium rather than nitrate. Current results highlight the hydrochemical controls on nutrient and phytoplankton dynamics in a small subtropical river reservoir under storms.

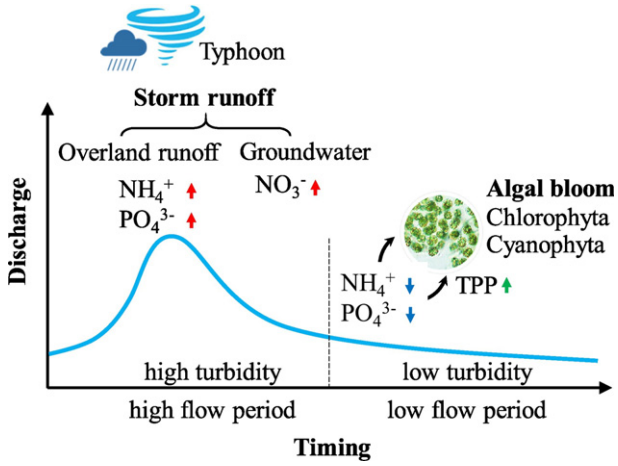


**Fig. 8.** A conceptual schematic of reservoir nutrient and phytoplankton in response to storms. Arrows indicate increase or decrease in nutrient concentrations.

## Acknowledgements

This research was partially supported by the National Natural Science Foundation of China (No. 41376082; 41573075), and the Fundamental Research Funds for the Central Universities (2012121053). We are grateful to T. Lu, X. Zhou, Z. Yan, and L. Wang who assisted in field work and lab analysis. We thank Jonathan Vause for his assistance with English editing.

## References

Akaike, H., 1974. A new look at the statistical model identification. IEEE Trans. Autom. Control 19, 716–723.
Becker, V., Huszar, V.L.M., Crossetti, L.O., 2009. Responses of phytoplankton functional groups to the mixing regime in a deep subtropical reservoir. Hydrobiologia 628, 137–151.
Bernal, S., von Schiller, D., Sabater, F., Martí, E., 2012. Hydrological extremes modulate nutrient dynamics in Mediterranean climate streams across different spatial scales. Hydrobiologia 719, 31–42.
Brooks, B.W., Lazorchak, J.M., Howard, M.D., Johnson, M.V.V., Morton, S.L., Perkins, D.A., et al., 2016. Are harmful algal blooms becoming the greatest inland water quality threat to public health and aquatic ecosystems? Environ. Toxicol. Chem. 35, 6–13.
Carpenter, S.R., Caraco, N.F., Correll, D.L., Howarth, R.W., Sharpley, A.N., Smith, V.H., 1998. Nonpoint pollution of surface waters with phosphorus and nitrogen. Ecol. Appl. 8, 559–568.
Casamayor, E.O., Schafer, H., Baneras, L., Pedros-Alio, C., Muyzer, G., 2000. Identification of and spatio-temporal differences between microbial assemblages from two neighboring sulfurous lakes: comparison by microscopy and denaturing gradient gel electrophoresis. Appl. Environ. Microbiol. 66, 499–508.
Chen, N., Wu, J., Hong, H., 2012. Effect of storm events on riverine nitrogen dynamics in a subtropical watershed, southeastern China. Sci. Total Environ. 431, 357–365.

Chen, N., Peng, B., Hong, H., Turyaheebwa, N., Cui, S., Mo, X., 2013. Nutrient enrichment and N:P ratio decline in a coastal bay-river system in southeast China: the need for a dual nutrient (N and P) management strategy. Ocean Coast. Manag. 81, 7–13.
Chen, N., Chen, Z., Wu, Y., Hu, A., 2014a. Understanding gaseous nitrogen removal through direct measurement of dissolved N-2 and N2O in a subtropical river-reservoir system. Ecol. Eng. 70, 56–67.
Chen, N., Wu, J., Chen, Z., Lu, T., Wang, L., 2014b. Spatial-temporal variation of dissolved N2 and denitrification in an agricultural river network, southeast China. Agric. Ecosyst. Environ. 189, 1–10.
Chen, N., Wu, Y., Chen, Z., Hong, H., 2015. Phosphorus export during storm events from a human perturbed watershed, southeast China: implications for coastal ecology. Estuar. Coast. Shelf Sci. 166, 178–188.
Chun, J.A., Cooke, R.A., Kang, M.S., Choi, M., Timlin, D., Park, S.W., 2010. Runoff losses of suspended sediment, nitrogen, and phosphorus from a small watershed in Korea. J. Environ. Qual. 39, 981–990.
Correll, D.L., Jordan, T.E., Weller, D.E., 1999. Effects of precipitation and air temperature on phosphorus fluxes from Rhode River watersheds. J. Environ. Qual. 28, 144–154.
Domingues, R.B., Barbosa, A.B., Sommer, U., Galvao, H.M., 2011. Ammonium, nitrate and phytoplankton interactions in a freshwater tidal estuarine zone: potential effects of cultural eutrophication. Aquat. Sci. 73, 331–343.
Erzini, K., 2005. Trends in NE Atlantic landings (southern Portugal): identifying the relative importance of fisheries and environmental variables. Fish. Oceanogr. 14, 195–209.
Gobler, C.J., Burson, A., Koch, F., Tang, Y.Z., Mulholland, M.R., 2012. The role of nitrogenous nutrients in the occurrence of harmful algal blooms caused by Cochlodinium polykrikoides in New York estuaries (USA). Harmful Algae 17, 64–74.
Hathaway, J.M., Tucker, R.S., Spooner, J.M., Hunt, W.F., 2012. A traditional analysis of the first flush effect for nutrients in stormwater runoff from two small urban catchments. Water Air Soil Pollut. 223, 5903–5915.
Heiskary, S.A., Walker, W.W., 1995. Establishing a chlorophyll a goal for a run-of-the-river reservoir. Lake Reservoir Manage. 11, 67–76.
Heisler, J., Glibert, P.M., Burkholder, J.M., Anderson, D.M., Cochlan, W., Dennison, W.C., et al., 2008. Eutrophication and harmful algal blooms: a scientific consensus. Harmful Algae 8, 3–13.
Hu, J., Liu, J.T., Liu, Y.D., 2009. Phosphorus in suspended matter and sediments of a hypertrophic lake. A case study: Lake Dianchi, China. Environ. Geol. 58, 833–841.
James, R.T., Havens, K.E., 1996. Algal bloom probability in a large subtropical lake. Water Resour. Bull. 32, 995–1006.
Joehnk, K.D., Huisman, J., Sharples, J., Sommeijer, B., Visser, P.M., Stroom, J.M., 2008. Summer heatwaves promote blooms of harmful cyanobacteria. Glob. Chang. Biol. 14, 495–512.
Jones, J.R., Knowlton, M.F., Obrecht, D.V., 2008. Role of land cover and hydrology in determining nutrients in mid-continent reservoirs: implications for nutrient criteria and management. Lake Reservoir Manage. 24, 1–9.
Kane, D.D., Conroy, J.D., Richards, R.P., Baker, D.B., Culver, D.A., 2014. Re-eutrophication of Lake Erie: correlations between tributary nutrient loads and phytoplankton biomass. J. Great Lakes Res. 40, 496–501.
Kuo, Y.M., Wu, J.T., 2016. Phytoplankton dynamics of a subtropical reservoir controlled by the complex interplay among hydrological, abiotic, and biotic variables. Environ. Monit. Assess. 188, 1–14.
Laine, A.O., Andersin, A.B., Leinio, S., Zuur, A.F., 2007. Stratification-induced hypoxia as a structuring factor of macrozoobenthos in the open Gulf of Finland (Baltic Sea). J. Sea Res. 57, 65–77.
Lu, T., Chen, N., Duan, S., Chen, Z., Huang, B., 2016. Hydrological controls on cascade reservoirs regulating phosphorus retention and downriver fluxes. Environ. Sci. Pollut. Res. 23, 24166–24177.
Luz Rodriguez-Blanco, M., Mercedes Taboada-Castro, M., Teresa Taboada-Castro, M., Oropeza-Mota, J.L., 2009. Nutrient dynamics during storm events in an agroforestry catchment. Commun. Soil Sci. Plant Anal. 40, 889–900.
Mamun, M., An, K.-G., 2017. Major nutrients and chlorophyll dynamics in Korean agricultural reservoirs along with an analysis of trophic state index deviation. J. Asia Pac. Biodivers. https://doi.org/10.1016/j.japb.2017.04.001.
Mo, Q., Chen, N., Zhou, X., Chen, J., Duan, S., 2016. Ammonium and phosphate enrichment across the dry–wet transition and their ecological relevance in a subtropical reservoir, China. Environ. Sci.: Processes Impacts 18, 882–894.
Molenat, J., Durand, P., Gascuel-Odoux, C., Davy, P., Gruau, G., 2002. Mechanisms of nitrate transfer from soil to stream in an agricultural watershed of French Brittany. Water Air Soil Pollut. 133, 161–183.
Nash, J.E., Sutcliffe, J.V., 1970. River flow forecasting through conceptual models part I — a discussion of principles. J. Hydrol. 10, 282–290.
Obermann, M., Rosenwinkel, K.H., Tournoud, M.G., 2009. Investigation of first flushes in a medium-sized Mediterranean catchment. J. Hydrol. 373, 405–415.
Ocampo, C.J., Oldham, C.E., Sivapalan, M., Turner, J.V., 2006. Hydrological versus biogeochemical controls on catchment nitrate export: a test of the flushing mechanism. Hydrol. Process. 20, 4269–4286.
Paerl, H., 2008. Nutrient and other environmental controls of harmful cyanobacterial blooms along the freshwater–marine continuum. Adv. Exp. Med. Biol. 619, 217–237.
Paerl, H.W., Gardner, W.S., Havens, K.E., Joyner, A.R., McCarthy, M.J., Newell, S.E., et al., 2016. Mitigating cyanobacterial harmful algal blooms in aquatic ecosystems impacted by climate change and anthropogenic nutrients. Harmful Algae 54, 213–222.
Parsons, T.R., Maita, Y., Lalli, C.M., 1984. Manual of chemical and biological methods for seawater analysis. Int. Rev. Hydrobiol. 70, 903–904.
Pearce, A.R., Chambers, L.G., Hasenmueller, E.A., 2017. Characterizing nutrient distributions and fluxes in a eutrophic reservoir, Midwestern United States. Sci. Total Environ. https://doi.org/10.1016/j.scitotenv.2016.12.168
Qiu, X., Huang, T., Zeng, M., 2016. Differences in phytoplankton dynamics and community structure between a wet year and dry year in the Zhoucun reservoir. J. Freshw. Ecol. 31, 377–391.
Reartes, S.B.R., Estrada, V., Bazán, R., Larrosa, N., Cossavella, A., López, A., et al., 2016. Evaluation of ecological effects of anthropogenic nutrient loading scenarios in Los Molinos reservoir through a mathematical model. Ecol. Model. 320, 393–406.
Rice, E.W., Baird, R.B., Eaton, A.D., Clesceri, L.S., 2005. Standard methods for the examination of water and wastewater, method 4500-CN-D: Titrimetric method. American Public Health Association, Washington, DC.
Santos, J.A., Marins, R.V., Aguiar, J.E., Challar, G., Silva, F.A., Lacerda, L.D., 2016. Hydrochemistry and trophic state change in a large reservoir in the Brazilian northeast region under intense drought conditions. J. Limnol. 76, 41–51.
Sims, J.T., Simard, R.R., Joern, B.C., 1998. Phosphorus loss in agricultural drainage: historical perspective and current research. J. Environ. Qual. 27, 277–293.
Sin, Y., Jeong, B., 2015. Short-term variations of phytoplankton communities in response to anthropogenic stressors in a highly altered temperate estuary. Estuar. Coast. Shelf Sci. 156, 83–91.
Smith, V.H., Joye, S.B., Howarth, R.W., 2006. Eutrophication of freshwater and marine ecosystems. Limnol. Oceanogr. 51, 351–355.
Søndergaard, M., Jensen, J.P., Jeppesen, E., 2003. Role of sediment and internal loading of phosphorus in shallow lakes. Hydrobiologia 506-509, 135–145.
Tweedley, J.R., Hallett, C.S., Warwick, R.M., Clarke, K.R., Potter, I.C., 2016. The hypoxia that developed in a microtidal estuary following an extreme storm produced dramatic changes in the benthos. Mar. Freshw. Res. 67, 327–341.
Tzoraki, O., Nikolaidis, N.P., Amaxidis, Y., Skoulikidis, N.T., 2007. In-stream biogeochemical processes of a temporary river. Environ. Sci. Technol. 41, 1225–1231.
Voynova, Y.G., Lebaron, K.C., Barnes, R.T., Ullman, W.J., 2015. In situ response of bay productivity to nutrient loading from a small tributary: the Delaware Bay-Murderkill Estuary tidally-coupled biogeochemical reactor. Estuar. Coast. Shelf Sci. 160, 33–48.
Wagner, L.E., Vidon, P., Tedesco, L.P., Gray, M., 2008. Stream nitrate and DOC dynamics during three spring storms across land uses in glaciated landscapes of the Midwest. J. Hydrol. 362, 177–190.
Wang, Y., Jiang, H., Jin, J.X., Zhang, X.Y., Lu, X.H., Wang, Y.Q., 2015. Spatial-temporal variations of chlorophyll-*a* in the adjacent aea area of the Yangtze River estuary influenced by Yangtze River discharge. Int. J. Environ. Res. Public Health 12, 5420–5438.
Webster, P.J., Holland, G.J., Curry, J.A., Chang, H.R., 2005. Changes in tropical cyclone number, duration, and intensity in a warming environment. Science 309, 1844–1846.
Wetzel, R.G., Likens, G.E., 2000. Limnological analyses. Springer, New York.
Woodward, G., Bonada, N., Brown, L.E., Death, R.G., Durance, I., Gray, C., et al., 2016. The effects of climatic fluctuations and extreme events on running water ecosystems. Philos. Trans. R. Soc. B 371, 20150274.
Wu, G., Xu, Z., 2011. Prediction of algal blooming using EFDC model: case study in the Daoxiang Lake. Ecol. Model. 222, 1245–1252.
Wu, L.G., Wang, B., Geng, S.Q., 2005. Growing typhoon influence on East Asia. Geophys. Res. Lett. 32.
Zhou, X., Chen, N., Yan, Z., Duan, S., 2016. Warming increases nutrient mobilization and gaseous nitrogen removal from sediments across cascade reservoirs. Environ. Pollut. 219, 490–500.
Zuur, A.F., Tuck, I.D., Bailey, N., 2003. Dynamic factor analysis to estimate common trends in fisheries time series. Can. J. Fish. Aquat. Sci. 60, 542–552.